8. W.K. De Logi and A.R. Mickelson, *Phys. Rev. D*, Vol. **16**, 10, 16, (1977) 2915 and references therein.
9. D. Fargion, "Gravitationally Induced Synchrotron Radiation: A New Test for General Relativity". Preprint 800 INFN 10/5/91, Rome, Italy; (and in these proceedings).
10. M.E. Gertsenstein, *Sov. Phys. JEPT.*, **14**, (1962) 84.
11. S. Weinberg, "Gravitation and Cosmology", by John Wiley & Sons Inc., (1972).
12. L.D. Landau and E.M. Lifshitz, *Field Theory*, Mir Moscow Ed. Riuniti, Italian Ed. (1976).
13. V.I. Ritus, *Sov. Phys. JEPT.*, **53**, (1981) 659.
14. A. Einstein, *Phys. Z.*, **18**, (1917) 121.
15. G.A. Schott, *Ann. Phys.*, Leipzig, **24**, (1907) 635.
16. A.A. Sokolov, I.M. Ternov, Synchrotron Radiation, Pergamon Press Ltd. (1968).
17. J. Schwinger, *Phys. Rev.*, **75**, (1949) 1912.
18. L.P. Grishchuk, *Sov. Sci. Rev. E. Astr. Space Phys.*, **7**, (1988), p. 267309.
19. K.S. Thorne, (1988) 300 Years of Gravitation, ed. S. Hawking and W. Israel, Cambridge Univ. Press (1990).
20. D. Gabor, "A New Microscopic Principle" Nature **161**, (1948) 777.
    R.J. Collier, C.B. Burckhardt and L.H. Lin, "Optical Holography", Academic Press 1971.
21. D. Fargion, "Acoustical Phase Conjugate Mirror", III. Int. Simp. on Holography, Lake Forest, Vol.**III**, T.Y. Jeong Ed., (1988) p. 345–349.

STUDY OF QED AT CRITICAL FIELD STRENGTH

IN INTENSE LASER–HIGH ENERGY ELECTRON COLLISIONS

K. T. McDonald
Joseph Henry Laboratories, Princeton University, Princeton, NJ 08544

C. Bamber[1], A. C. Melissinos[1] and D. Meyerhoffer[2]
Department of Physics[1], Department of Mechanical Engineering[2], University of Rochester, Rochester, NY 14627

P. Chen and J. E. Spencer
Stanford Linear Accelerator Center, Stanford University, Stanford, CA 94309

R. B. Palmer
Stanford Linear Accelerator Center, Stanford, CA 94309 and Brookhaven National Laboratory, Upton, NY 11973

ABSTRACT

We propose a program of study of the interaction of electrons and photons in fields approaching the critical QED field strength of an electron rest energy per Compton wavelength. This can be achieved in collisions between the picosecond pulses of a teraWatt laser and a 50-GeV electron beam. The phenomena accessible to study include nonlinear Compton scattering, trident production, and Breit-Wheeler pair production. The electric field at the laser focus is of similar strength to that of an electron bunch in future linear colliders, permitting a close analog of beamstrahlung to be studied. Measurement of the invariant-mass spectrum of electron-positron pairs could clarify whether the positron peaks seen at Darmstadt in heavy-ion collisions are a strong-field QED effect. Electron-laser collisions at critical field strength may prove to be a high-brightness source of positrons for future colliders.

1 Introduction

We propose to study the scattering of 50-GeV electrons from a focused short pulse of UV light ($\lambda = 350$ nm) with peak energy flux $I \sim 4 \times 10^{17}$ W/cm^2. At this energy density, the ratio of the electric field $E^\star = \gamma E$ seen by the electron[1] to the Schwinger critical field [1],

$$\Upsilon \equiv \gamma \frac{eE\hbar}{m^2c^3}, \tag{1}$$

approaches unity. At such fields perturbative QED loses its validity and one expects copious production of e^+e^- pairs through multiphoton absorption [2].

More generally, multiphoton effects become important in a wave field of frequency ω when the parameter

$$\eta \equiv \frac{eE}{\omega mc} \tag{2}$$

approaches or exceeds unity. This (Lorentz invariant) parameter is proportional to magnitude of the classical vector potential of the wave field, and characterizes the transverse velocity induced on an electron by the wave. When this velocity approaches c higher multipole radiation predominates, corresponding to multiphoton absorption in a quantum description. Multiphoton-absorption processes have been observed with atomic electrons but not with high-energy free electrons.

If the incident wave is circularly polarized, then the electron's motion is a circle of radius r in the frame in which the electron has no longitudinal velocity. We introduce a transverse velocity $\beta_\perp$ and a transverse relativistic factor $\gamma_\perp$ through

$$eE = \gamma_\perp m\omega^2 r = \gamma_\perp \beta_\perp m\omega c, \tag{3}$$

where

$$\beta_\perp = \frac{v_\perp}{c} = \frac{\omega r}{c} \qquad \gamma_\perp = \left(1 - \beta_\perp^2\right)^{-1/2}. \tag{4}$$

Therefore the parameter η of Eq. (2) can be written as

$$\eta = \gamma_\perp \beta_\perp \qquad \text{and} \qquad \gamma_\perp = \left(1 + \eta^2\right)^{1/2}. \tag{5}$$

Due to its transverse motion in the field the electron acquires an "effective mass"

$$\overline{m}^2 = m^2\gamma_\perp^2 = m^2\left(1 + \eta^2\right). \tag{6}$$

[1]Strictly speaking, $E^\star = 2\gamma E$ for a wave field, but it is conventional to leave out the factor of 2 in the definition of Υ.

In a quantum description one does not refer to the classical path of the transverse motion of the electron in the wave field, but rather the Volkov solutions to the Dirac equation [3]. The kinematic character of these solutions can be summarized by writing the four-vector of the electron as

$$\overline{p}_\mu = p_\mu + \kappa\omega_\mu, \tag{7}$$

where p_μ is the four-vector of the electron in the absence of the wave, ω_μ is the four-vector of a wave photon, and $\kappa = \eta^2 m^2/2(p\cdot\omega)$. The latter relation follows from setting $\overline{p}^2 = \overline{m}^2$. Loosely speaking, an electron in a wave field has absorbed κ wave photons. If an electron or positron is created in the field, its invariant mass is immediately $\overline{m}$, which relaxes to m only when the particle leaves the wave field.

In the proposed studies of strong-field QED we will simultaneously explore the two nonlinear effects of multiphoton absorption, and of vacuum polarization. While the case of $\eta \approx 1$ can be realized in low-amplitude, long-wavelength fields, the Schwinger parameter Υ can approach 1 with present day lasers only when probed with electrons of 50-GeV energy. In principle, $\Upsilon \sim 1$ can also be reached in heavy-ion collisions [4] when the Z of the combined nuclei satisfies $\alpha Z > 1$, and in channeling of very high-energy electrons through thin crystals [5]. Beamstrahlung at future linear colliders is another situation in which Υ can exceed unity unless the beam parameters are suitably chosen.

Our proposal involves four related measurements which can be carried out in the A-line (upgraded to 50 GeV), or in the C line. All four experiments use the same apparatus with minor modifications and are a natural progression in a systematic test of QED at critical field strength. The experiments are of increasing complexity and their goals are correspondingly more ambitious, as follows:

(a) Nonlinear (multiphoton) Compton scattering. For this experiment we can use an infrared laser ($\lambda = 1,054$ nm) and the demands on the electron beam are minimal. Apart from its intrinsic interest, this experiment is also a pilot for the generation of an intense high-energy gamma beam needed for measurements (c) and (d). This work would be a continuation of an ongoing program now underway at BNL [6].

(b) Measurement of the energy and transverse momentum distributions of the high-energy γ's and e^+e^- pairs produced by multiphoton absorption. Namely, an experimental study of the beamstrahlung process [7] at values of Υ typical of the next generation of linear colliders. As in the previous measurement, IR or UV laser pulses can be used.

(c) We wish to measure pair production in γ-γ scattering with both photons real:

$$n\omega_0 + \omega \rightarrow e^+e^-. \quad (8)$$

This is the multiphoton version of the Breit-Wheeler process [8] where ω_0 are the incident laser photons and ω is a high-energy photon derived from backscattering the laser photons ω_0 off the electron beam [9, 10]. We will use a UV (λ = 350 nm) pulse, which yields high-energy photons ω_{max} = 36.5 GeV. The expected flux in the upper 10% of the energy band is $\gtrsim 10^5$/pulse. Part of the UV pulse is brought in collision with the electrons to produce the high-energy photons, whereas the other half of the UV is tightly focused and brought in collision with the high-energy photons. For a UV laser at SLAC, we need to absorb at least three laser photons to make an e^+e^- pair.

(d) The mass spectrum of the e^+e^- pairs produced in reaction (8) is of special interest and can be measured with a resolution of 10 keV in the low-mass region, $M \sim 1.0$-2.0 MeV/c^2. This is the region where the Darmstadt experiments have observed peaks in the e^+e^- effective mass [4]. The only possible explanation for this structure is that it is associated with the high fields present during the heavy-ion collision; similar field strengths are present in our experiment. Two experiments have demonstrated that there are no resonances in e^+e^- scattering in a field-free region [11, 12]. Some authors have speculated that at high fields QED undergoes a phase transition to a confining state, which would have bound e^+e^- states [13]. Our experiment offers the best opportunity at the present time to test these conjectures in the laboratory free from the complications of the strong interaction.

The production of positrons by direct pair production in multiphoton-electron interactions, or by multiphoton-electron scattering followed by reaction (8) [14] could have a major impact on the performance of future linear e^+e^- colliders. The luminosity of such colliders is limited by the brightness of the electron and positron sources used, and these, in present designs, are limited by the brightnesses that can be generated in damping rings. Electrons of greater brightness can be generated in rf photocathode guns but if positrons are made from the electrons by pair production in targets then their emittance is relatively large. A damping ring must then be used, at least for the positrons, and this limits the luminosity. If multiphoton-electron interactions are used to generate the positrons at a strong electron focus then their emittance will be little greater than that of the initial electrons, the brightness will be substantially preserved, no damping rings would be required and the potential luminosity of the collider could be raised.

In the next section we discuss the general layout of the experiment, *i.e.*, of the interaction region and of the detector. This is followed by a discussion of each of the four proposed measurements. A brief review of the laser system which we have developed for this experiment is given in the closing section.

2 Experimental Setup

A schematic representation of the experimental layout is shown in Fig. 1. The electron-photon interaction point is chosen in a region where the beam is practically parallel. This is because for measurements (a,b) the event rate is more than adequate and there is no need to focus the electron beam. Furthermore a parallel beam allows the measurement of the angular distribution of the backscattered γ's with good accuracy. For measurements (c,d) the electron beam must have small angular divergence so that the produced γ's can be transported to the next interaction point without large geometric losses. In fact it can be shown that to first approximation, the luminosity of the γ-ω collisions is independent of the focusing strength (β^*) of the primary electron beam; see Eq. (12), and the Appendix.

The primary interaction point should be followed by a magnetic region to deflect the electron beam and to sweep away charged secondary particles. The dog-leg shown in Fig. 1 restores the electron beam to its original direction whereas the backscattered γ's emerge at 24 mrad. The typical intensity of the γ-beam is $\sim 10^5$ per laser pulse.

The detector is a magnetic pair spectrometer with moderate field integral yielding $P_\perp = 0.25$ GeV/c. We will use silicon strip counters to measure the e^+e^- momenta, and a thin silicon strip counter to convert the γ's and measure the production angle. A small Pb-glass array behind the final counters will be used to check the measured momenta and reject ambiguities. The detector is shown schematically in Fig. 2.

In the first two measurements (a,b) the flux through the detector is kept below 10^3 γ/pulse since it is important to reject events where two conversions occur in the same pulse. For measurements (c,d) which involve the detection of e^+e^- pairs produced directly in γ-ω collisions a flux of 10^5 γ/pulse traverses the center of the spectrometer. Thus, all material is removed from the forward direction and we rely on the bending of the e^+e^- to detect them outside the beam region.

The detector is located approximately 30 m from the e-ω interaction point. Assuming a 20-μm pitch for the counters, the angular resolution is of order $\Delta\theta \sim 7\times10^{-7}$ rad. The angular distribution of the backscattered γ's is in the range $\theta \sim 10^{-5}$ rad; thus it can be adequately measured provided the electron beam divergence is kept at the level of $\sigma_\theta \sim 10^{-6}$. The interaction products are transported to the spectrometer in vacuum; a small aperture (2-inch) beam pipe is adequate.

We assume that in general the laser beam will be focused to an area smaller than the electron beam. To achieve $\Upsilon \sim 1$ the laser beam must be focused as tightly as possible. This implies an optical system with small values of f/D and for practical

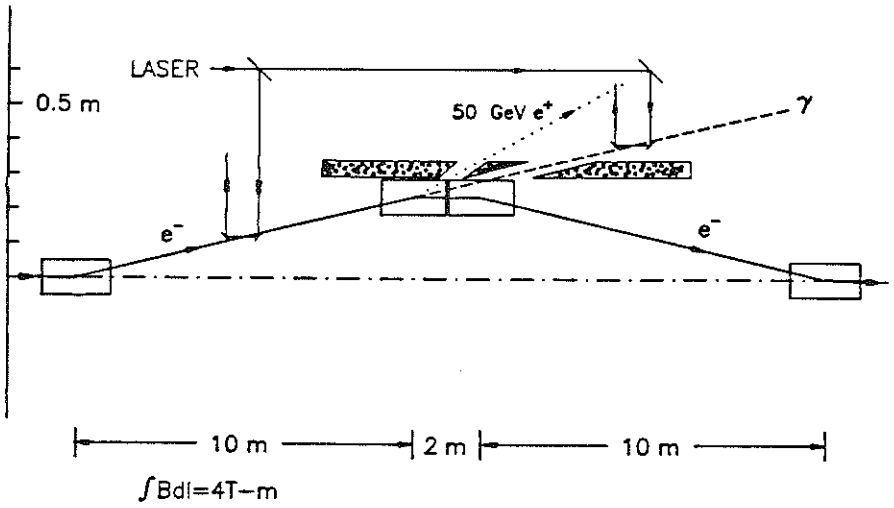

Figure 1: Layout of the experiment.

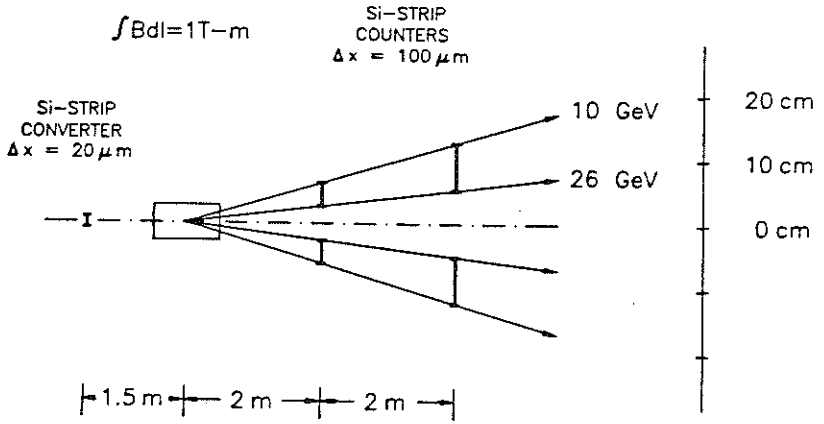

Figure 2: Schematic of the magnetic pair-spectrometer detector.

reasons we choose $f/D \sim 3$. To retain a small crossing angle, the electron beam will pass through a hole in the final mirror. We have chosen a small crossing angle, $\delta \lesssim 10$ mrad, in order to simplify the synchronization of the laser and electron pulses which are of comparable longitudinal dimensions: $\sigma_e \sim 500\,\mu$m, $\sigma_\omega = 50$-$500\ \mu$m, where the lower limit on σ_ω is for a tightly focused beam. The synchronization is achieved by locking the laser oscillator "mode-locking" crystal frequency (100 MHz) to that of the linac r.f. A 1° phase angle in the electron beam corresponds to 1-ps jitter, which is of the order of the laser pulse length. σ_ω as given above is determined by the smaller of the confocal parameter $z_0 = 2.28\,\lambda\,(f/D)^2$, or pulse length. Our present laser system is operating with a repetition rate of 0.25 to 0.05 Hz [15]. However the system will be improved and all event rates are based on a 1-Hz cycle.

For the electron beam we assume the following parameters

$$\begin{aligned} \text{Invariant emittance } \gamma\epsilon &= 3\times10^{-5}\text{ m-rad} \\ \text{Electron energy} &= 50\text{ GeV} \\ \text{Electrons per pulse} &= 10^9\text{-}10^{10} \\ \text{Bunch length} &= 500\ \mu\text{m} \end{aligned}$$

It is preferable to operate with the electron beam quasiparallel and we assume $\sigma_\theta = 10^{-6}$ which leads to $\sigma_\tau = 300\ \mu$m. The rate of backscattered high energy γ's can be estimated from

$$N_\gamma = \frac{N_e}{A_e}\,\sigma_c\,N_L, \tag{9}$$

where

$$\begin{aligned} N_e &= \text{Number of electrons in bunch} \\ A_e &= \text{Area of electron bunch} \\ N_L &= \text{Number of photons in laser pulse} \\ \sigma_c &= \text{Compton cross section} \end{aligned}$$

For a UV pulse of energy 0.05 J, $N_L = 10^{17}$; $\sigma_c \simeq 2.5\times10^{-25}$ cm^2; and if we take $A_e = \pi\sigma^2$ with $\sigma = 300\mu$m, we obtain $N_\gamma/N_e \approx 10^{-4}$. This rate is more than adequate for measurements (a,b) and it may be necessary to reduce the beam intensity to avoid multiple events in the detector.

Note that the transverse dimensions of the backscattered high-energy γ beam are those of the focused laser spot, that is of the order of a 100 μm. Furthermore the high-energy part of the γ beam follows the direction of the electron beam and therefore remains parallel to a few parts in 10^{-6}. For example, the small-angle approximation to the exact kinematic relation (14) is

$$E_\gamma \approx \frac{4\gamma^2\omega_0}{1+4\gamma\omega_0/m+(\gamma\theta)^2} = \frac{36.5\text{ GeV}}{1+(\gamma\theta/1.95)^2}, \tag{10}$$

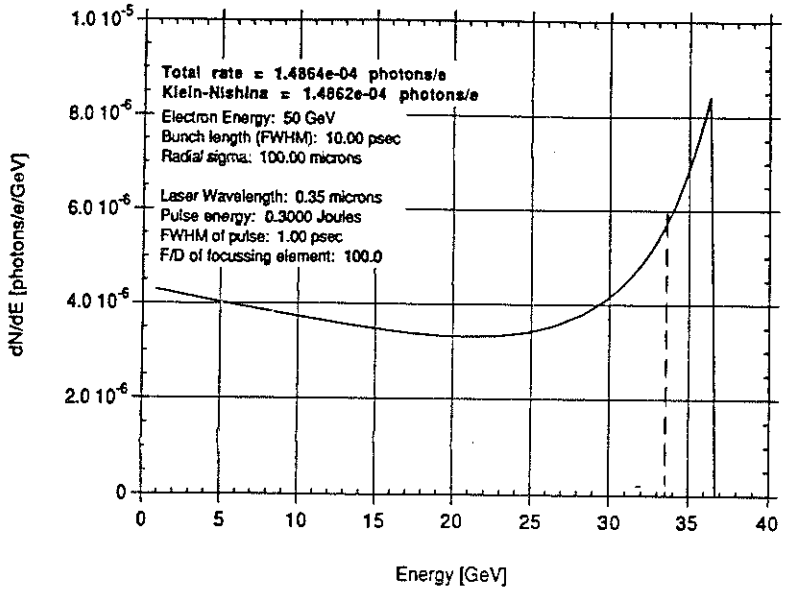

Figure 3: The spectrum of the backscattered photons when a laser pulse of $\lambda = 350$ nm is incident on 50-GeV electrons.

for a 50-GeV electron beam colliding with a laser pulse of wavelength 0.351 μm. The energy spectrum of the scattered γ's is shown in Fig. 3, where the dashed line indicates the limiting energy for γ's scattered at an angle smaller than $\theta = 6 \times 10^{-6}$ rad; this region contains energies within 9% of the peak energy.

To scatter the high-energy γ's off the focused laser beam a second interaction point is chosen. This is shown in Fig. 1 at a distance of $L = 10$ m from the production point of the γ's. In traveling from the production point to the γ-ω interaction region the high-energy γ's will be spread out due to the geometric divergence (or convergence) of the parent electron beam and also because of the scattering angle. If we wish to accept at the second interaction region an energy bite ΔE, we must accept a range of Compton scattering angles $\Delta\theta$, where

$$\left(\frac{\gamma\Delta\theta}{1.95}\right)^2 = \frac{\Delta E}{E}, \tag{11}$$

according to Eq. (10). This implies that the e-ω interaction should take place over a region of radius at least $L\Delta\theta$.

The luminosity (per laser pulse) at the second (γ-ω) interaction region can be calculated as in Eq. (9) since the laser beam is tightly focused here,

$$\mathcal{L} = \frac{N_\gamma}{A_\gamma}\frac{\Delta E}{E}\frac{N_L}{2} = \frac{N_\gamma (N_L/2)^2}{A_e A_\gamma}\frac{\Delta E}{E}\sigma_c. \tag{12}$$

In this, N_γ are the γ's produced at the first interaction region, and they are contained in an area A_γ at the second interaction region. $\Delta E/E$ is the energy bite and we assume a uniform distribution in energy (which underestimates the luminosity according to Fig. 3). Finally we assume that half of the laser photons are used at each of the interaction regions.

We estimate A_γ from

$$A_\gamma \approx \pi\sigma_{r_2}^2 = \pi(L\Delta\theta)^2.$$

For the nearly parallel beam we are considering, A_e in Eq. (9) is almost the same as A_γ, but it is insightful to write this as

$$A_e \approx \pi\sigma_{r_2}^2 \approx \pi\frac{\epsilon^2}{\sigma_\theta^2} \approx \pi\frac{\epsilon^2}{\Delta\theta^2},$$

which introduces the emittance of the electron beam in the relevant manner. See the Appendix for more detailed considerations.

Inserting these factors in Eqs. (9,12) we obtain

$$\mathcal{L} = \frac{N_e (N_L/2)^2}{\pi^2\epsilon^2 L^2}\frac{\Delta E}{E}\sigma_c. \tag{13}$$

The quantity N_e/ϵ^2 is the brightness of the electron beam.

Using the parameters already mentioned

$$\begin{aligned} N_e &= 10^{10} \\ N_L &= 2 \times 10^{17} \\ \epsilon &= 3 \times 10^{-10} \text{ m-rad} = 3 \times 10^{-8} \text{ cm-rad} \\ L &= 10 \text{ m} = 10^3 \text{ cm} \\ \Delta E/E &= 0.09 \\ \sigma_c &= 2.5 \times 10^{-25} \text{ cm}^2 \end{aligned}$$

we find

$$\mathcal{L} \approx 2 \times 10^{26} \text{ cm}^{-2}\text{s}^{-1}.$$

The estimated cross section for $\gamma + n\omega \to e^+e^-$ at our energies is of order $\sigma \sim 10^{-27}$ cm^2 (see Sec. 5 below) so that the event rate is comfortable. Recall that we cannot use more than one event per laser pulse. The luminosity can be further increased by increasing N_e or N_L, or by decreasing ϵ or L. The number of high-energy γ's participating in the second interaction is $N_\gamma\Delta E/E \approx 3 \times 10^5$.

3 Nonlinear Compton Scattering

Backscattering of a low-energy photon ω_0 from a high-energy electron beam results in an energetic gamma ray moving along the electron beam's direction [9]. The energy of the gamma ray is given by

$$\omega = \omega_0 \frac{4\gamma^2}{1 + 2\gamma^2(1-\cos\theta) + (2\gamma\omega_0/m)(1+\cos\theta)} \tag{14}$$

where $E_e = \gamma m$ is the electron energy and θ is the laboratory scattering angle, which is of order $1/\gamma$. It is convenient to introduce the dimensionless parameters [1]

$$x = 4\omega_0 E_e/m^2, \qquad y = \frac{\omega}{E_e} \le y_{max} = \frac{x}{1+x}. \tag{15}$$

The differential cross section is then given by

$$\frac{d\sigma}{dy} = \frac{2\pi r_0^2}{x}\left[(1-y) + \frac{1}{(1-y)} - \frac{4y}{x(1-y)} + \frac{4y^2}{x^2(1-y)^2}\right] \tag{16}$$

with $r_0 = e^2/m = 2.82 \times 10^{-13}$ cm the classical electron radius. For $x > 2$ the total cross section can be approximated by

$$\sigma_C = \frac{2\pi r_0^2}{x}\left(\ln x + \frac{1}{2}\right). \tag{17}$$

In intense fields, the above equations are modified because of multiphoton absorption and of the transverse mass of the electron. Thus the energy of the backscattered photon is given by

$$\omega = n\omega_0 \frac{4\gamma^2}{1 + 2\gamma^2(1-\cos\theta) + [2n\gamma\omega_0/m + \eta^2/2](1+\cos\theta)} \tag{18}$$

The differential cross section can be given in closed form when the incident photons are circularly polarized [16]:

$$\frac{d\sigma_n}{dy} = \frac{2\pi r_0^2}{x}\left\{-\frac{4}{\eta^2}J_n^2(z) + \left(2 + \frac{u^2}{1+u}\right)\left[J_{n-1}^2(z) + J_{n+1}^2(z) - 2J_n^2(z)\right]\right\} \tag{19}$$

In the above equations the index n labels the number of photons absorbed from the field of the laser and the parameters u, z are defined through

$$u \simeq \frac{y}{1-y}, \qquad y_{\max} = \frac{nx}{1+\eta^2+nx}, \qquad z = \eta\sqrt{1+\eta^2}\,\frac{2}{x}\sqrt{u\left(\frac{nx}{1+\eta^2} - u\right)}. \tag{20}$$

In Fig. 4 we show the differential cross section for

$$\begin{aligned} E_e = \gamma m &= 50 \text{ GeV} \\ \omega_0 &= 1.17 \text{ eV } (\lambda = 1{,}054 \text{ nm}) \\ \eta &= 0.4 \end{aligned}$$

Numerically

$$\eta^2 = \left(\frac{eE}{m\omega c}\right)^2 = 0.4\left[\frac{I}{10^{18}\ \mathrm{W/cm^2}}\right]\left[\frac{\lambda}{1.054\ \mu\mathrm{m}}\right]^2 \tag{21}$$

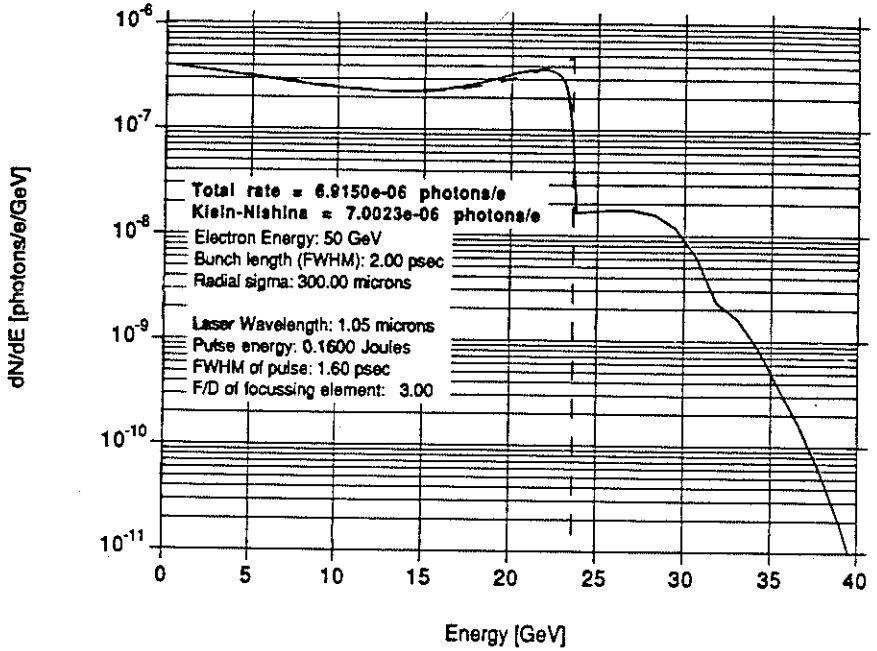

Figure 4: Differential cross section for multiphoton scattering of a $\lambda = 1{,}054$ nm laser pulse from 50-GeV electrons.

We take the energy in the laser pulse to be $\mathcal{E} = 0.12$ J and the width $\Delta t = 1.2$ ps. The pulse is brought to a focus with radius $R = 2.8\ \lambda$, to yield a flux $I = 4 \times 10^{17}$ W/cm^2, which results in $\eta = 0.4$. These parameters are conservative and have been achieved in the laboratory [15]. The corresponding photon density at the focal point is

$$N_\omega/\mathrm{cm}^2 = I\Delta t/\omega_0 = 2.6 \times 10^{24}\ \text{photons/cm}^2$$

[This equals the electron density in a 1-cm-thick sheet of lead.]

The laser pulse is brought into collision with the electron beam at an angle $\Delta = 10^{-2}$ rad as shown in Fig. 1. For the electron beam we assume the parameters discussed in section 2. The rate of backscattered photons has been calculated by convoluting the two beam distributions with the cross section given by Eq. (19). We find that

$$N_\gamma \sim 10^3/\text{interaction}$$

with energy $E_\gamma > 6$ GeV. The photons are contained within an angle $\theta < \sqrt{2}/\gamma$ which includes the electron beam divergence and the scattering angle. The photons travel to the detector located at 30 m from the interaction point in a vacuum pipe of modest dimensions (2-inch diameter).

A small fraction of the backscattered photons ($\sim$ 0.5 %) is converted in a thin Si-strip detector with good spatial resolution (20-μm pitch) and the produced pair is analyzed by a dipole magnet with transverse kick $P_\perp = 0.3$ GeV/c (1 T-m). To provide adequate acceptance for asymmetric conversions we use small drift chambers to measure the electron and positron tracks after the magnet. The chambers are 30-cm long and are separated by 2 m as shown in Fig. 2; they have a resolution of $\Delta x = 200$ μm. A small lead-glass array behind the tracking chambers provides a coarse check of the energy and is used to reject background. The acceptance of the spectrometer is shown in Fig. 5 and falls off for $E_\gamma < 6$ GeV. The energy resolution is $\Delta E_\gamma < 0.01\, E_\gamma$.

In this measurement only one γ can be detected per pulse, and this is why the thin converter is used. We would like to operate with an event rate of 0.5 conversions per pulse. Since the laser beam intensity and focal properties are set by the desired value of η the event rate must be controlled by attenuating or by defocusing the electron beam. We wish to accumulate 200 events in the third harmonic which implies collecting 50,000 γ's. This corresponds to one day's running at 1-Hz pulse rate and 0.5 events/pulse. The data should also allow us to observe the shift of the end-point of the first harmonic due to the electron's transverse mass.

This experiment will be among the first observations of multiphoton Compton scattering. By varying η the effect of laser beam intensity on the cross section can be studied. The experiment will also provide us with the necessary experience on the mutual alignment of the beams and of their time-synchronization. The information on the yield and spectral quality of the backscattered photons is, of course, necessary for the design of the γ-γ scattering experimental setup.

4 Beamstrahlung

Of primary interest in the design of future linear colliders is the degradation of the primary beams due to beamstrahlung. In addition, low-energy e^+e^- pairs produced

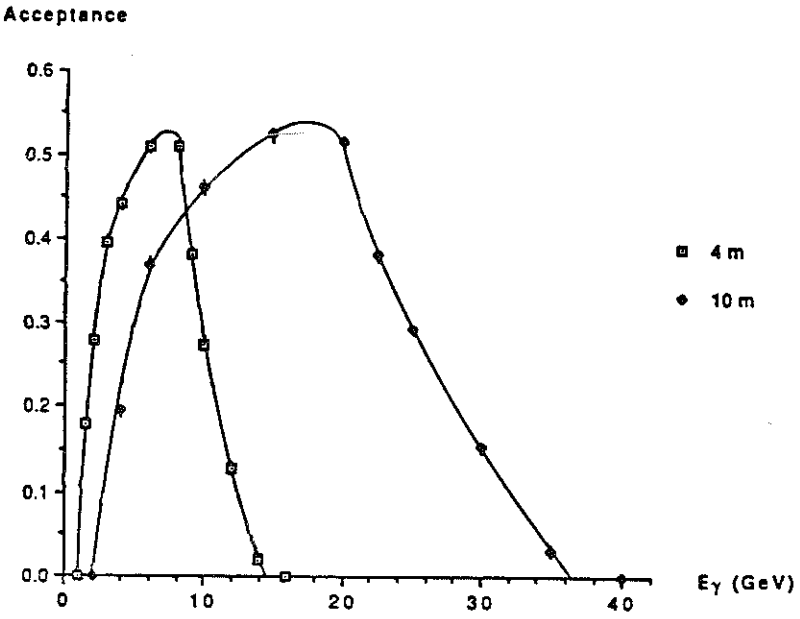

Figure 5: The spectrometer acceptance.

by beamstrahlung can result in serious background in the detector. Our experimental set-up makes it possible to test some of these predictions because the electrons passing through the laser focus see a near-critical field. In the multiphoton Compton experiment, the intensity parameter was set at $\eta = 0.4$ which corresponded to $\Upsilon = 0.1$. [Note that $\Upsilon = \eta x/4$.] For the beamstrahlung we expect to work at $\Upsilon = 0.3$; this can be achieved by increasing the energy in the laser pulse, while also focussing more tightly, reaching peak values of $\eta = 1.2$.

The fractional energy loss of an electron in a high field is given by Chen and Yokoya [17] as

$$\varepsilon = \frac{I}{E_e} = \frac{\sqrt{\pi}}{3}\frac{\alpha\sigma_z}{\lambda\!\!\!^{-}_c\gamma}\Upsilon^2 \qquad \Upsilon \ll 1. \tag{22}$$

Using $\sigma_z = 0.03$ cm, we find for $\Upsilon = 0.1$ that $\varepsilon = 0.3$. Thus the electrons that cross the laser focus will lose substantial energy; if $\Upsilon = 0.3$, ε is of order unity. Such energy losses can be best measured by calorimetric methods.

We plan to measure the produced γ's over a range of angles outside the cone of

direct (single-photon) production. This will cover the range from 1 to 10 mrad using a small silicon-strip calorimeter with tungsten absorber plates. The overall dimensions are 6×6 cm^2 and the read out pitch is 200 μm for x and y coordinates; the calorimetry is performed by 8 silicon planes which are read out for the total energy deposited. Such a device [18] has a demonstrated energy resolution $\Delta E_\gamma / E_\gamma = 0.24/\sqrt{E_\gamma}$ in the range $E_\gamma \sim 20$ GeV. Assuming a lower cut off of 3 GeV, the angular range covers the $P_\perp$ range from 0.030 to 0.500 GeV/c. While it is not evident that $P_\perp$ is the characteristic parameter in this process, $P_\perp$ is invariant with respect to the choice of longitudinal reference frame. Large $P_\perp$ is clearly a manifestation of multiphoton absorption.

For pair production in intense fields we follow Chen and Telnov [19] who give the number of pairs per electron as

$$n_p = \frac{4\sqrt{3}}{25\pi} \left[\frac{\alpha \sigma_z}{\gamma \lambda\!\!\!^{-}_c} \Upsilon \right]^2 \Xi(\Upsilon) \qquad \Upsilon \ll 1 \tag{23}$$

As before σ_z is the length of the laser focal region, and the function $\Xi(\Upsilon)$ decreases exponentially for $\Upsilon < 1$. For $\Upsilon = 0.3$, $\gamma = 10^5$ and $\sigma_z = 0.03$ cm,

$$n_p = 2.3 \times 10^{-5},$$

assuring adequate rate.

Experimentally it is easiest to measure the high end of the positron spectrum. The positrons are dispersed by the second bending magnet and clearly separated from the photons. By translating the spectrometer magnet we can cover the momentum range $25 < P_{e^+} < 50$ GeV/c in three steps. If it is desirable to measure the low-energy positron spectrum a larger area detector closer to the dispersing magnet will be needed.

5 The Multiphoton Breit-Wheeler Process

We wish to investigate pair production by real photons

$$n\omega_0 + \omega \rightarrow e^+ e^- \tag{24}$$

As mentioned in the introduction we use a UV pulse to create the photon beam which has the spectrum shown in Fig. 3. The beam is brought into collision with the remainder of the UV pulse which is now focused to high intensity ($\eta = 1.2$) to make multiphoton absorption probable.

Pair creation by n laser photons is the cross-channel process from nonlinear Compton scattering, and for circular polarization of both the laser photons and the high-energy photon is given in analogy to Eq. (19) by [16]

$$\frac{d\sigma_n}{dy} = \frac{2\pi r_0^2}{x} \left\{ \frac{4}{\eta^2} J_n(z) + (u-2) \left[J_{n-1}^2(z) + J_{n+1}^2(z) - 2J_n^2(z) \right] \right\} \tag{25}$$

where (for $n\omega_0 \ll \omega$)

$$x = \frac{4\omega_0 \omega}{m^2}, \qquad y = \frac{E_e}{\omega}, \qquad y_{\max,\min} = \frac{1}{2} \pm \sqrt{\frac{1}{4} - \frac{1+\eta^2}{nx}}, \qquad u = \frac{1}{y(1-y)}, \tag{26}$$

and z is defined as before. The cross section exists only for those values of n such that $y_{\max}$ is real.

The cross section for reaction (24) for $\eta = 0.4$ and $\omega_0 = 3.5$ eV, is shown in Fig. 6 as a function of the energy of the γ. The thresholds for pair production via n laser photons are given by

$$E_n = \frac{m^2(1+\eta^2)}{n\omega_0}. \tag{27}$$

The thresholds for $n = 1$ at 86.2 GeV, $n = 2$ at 43.1 GeV, and $n = 3$ at 28.7 GeV are visible in the Figure. For γ's from Compton backscatter from a 50-GeV electron beam, the maximum energy is 36.5 GeV at which energy three laser photons are required for pair production. The cross section reaches a maximum of 1.6×10^{-25} cm^2 for $E_\gamma \approx 155$ GeV. At this energy the pair-production cross section is almost the same as the Compton cross section, so pair production would be very prominent.

Figure 7 illustrates the nonlinear dependence of the pair-production cross section on the laser field strength. It varies as η^4 for weak fields, but saturates at $\eta \approx 1.5$.

Figure 8 shows the differential cross section for pair production as a function of the lab energy of the electron or positron. For the parameters considered, the electrons are nonrelativistic in the pair rest frame, so the lab energies do not extend down to zero or up to the incident-γ energy. The kink in the curve corresponding to $\eta = 0.4$ is at the transition between dominance by three and by four laser photons.

Since reaction (24) has not been observed with real photons it is of interest to confirm the cross section and this is the goal of the present measurement. The pairs are moving in the forward direction and have a very small opening angle. The e^+e^- are detected by a high resolution Si-strip detector with 10-20 μm resolution and their momentum measured in the spectrometer magnet.

The mass resolution is evaluated from

$$M^2 \simeq 4m^2 + P_+ P_- \theta^2 \tag{28}$$

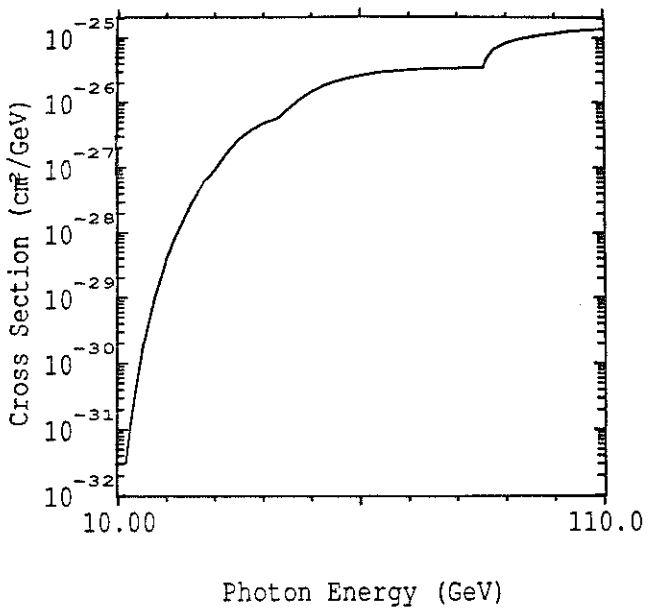

Figure 6: Total cross section for pair production when high-energy photons are incident on a $\lambda = 350$ nm laser pulse with field strength $\eta = 0.4$. The thresholds for production via 1, 2, and 3 laser photons are visible at 86.2, 43.1, and 28.7 GeV, respectively.

with θ the opening angle and P_+, P_- the positron and electron momenta. For symmetric decays, $P_+ \sim P_- \sim 20$ GeV so that $\theta \sim 3 \times 10^{-5}$ at $M = 1.2$ MeV. Since

$$\sigma_M = \frac{M^2 - 4m^2}{2M} \sqrt{2\left(\frac{\sigma_P}{P}\right)^2 + \left(\frac{\sigma_\theta}{\theta}\right)^2} \tag{29}$$

we wish to measure θ and P_+, P_- to $\sim 2\%$ accuracy. This implies $\sigma_\theta \sim 6 \times 10^{-7}$ which corresponds to $\Delta x = 18\,\mu$m at 30 m. For the charged-particle momenta, we note that the incident direction is known with the precision $\Delta\theta$ and will be smeared by multiple scattering in the 300-μm-thick Si-strip detector. This contributes a transverse kick of 1 MeV/c, which is quite acceptable given the transverse kick $P_\perp = 300$ MeV/c in the analyzing magnet.

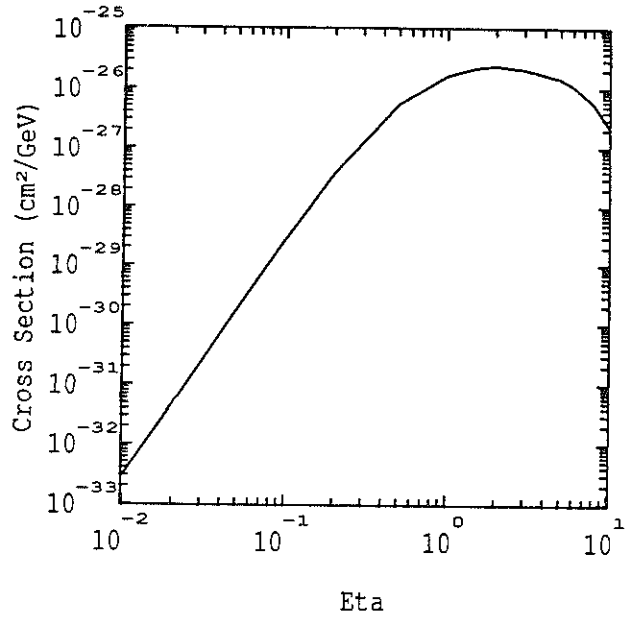

Figure 7: Total cross section for pair production when 36.5-GeV photons are incident on a $\lambda = 350$ nm laser pulse of field strength η.

The technical difficulty with this setup is that a fraction of the high-energy photon beam ($N_\gamma = 10^3$/pulse) passes through the middle of the detector. Thus the Si-strip counter should be made as thin as possible, hopefully down to 100 μm which corresponds to a conversion probability of 10^{-3}. If this problem cannot be resolved, we will forego the direct measurement of the opening angle, and infer it from the tracking.

The rate for this process is slower. Given an effective cross section for 2-photon absorption

$$\sigma_{(3\omega_0 + \omega' \to e^+e^-)} \simeq 10^{-27}\ \text{cm}^2$$

and a photon density of 10^{24}/cm^2 the pair-production probability is 10^{-3}. The high-energy-photon flux is estimated at 10^4/pulse. Depending on the focal properties of the electron beam, 10% of these high-energy photons will cross through the laser focus. We assume another factor of 10 for selection of symmetric pairs and detection efficiency in the presence of the high-energy photon beam. Thus we expect 1 pair/10

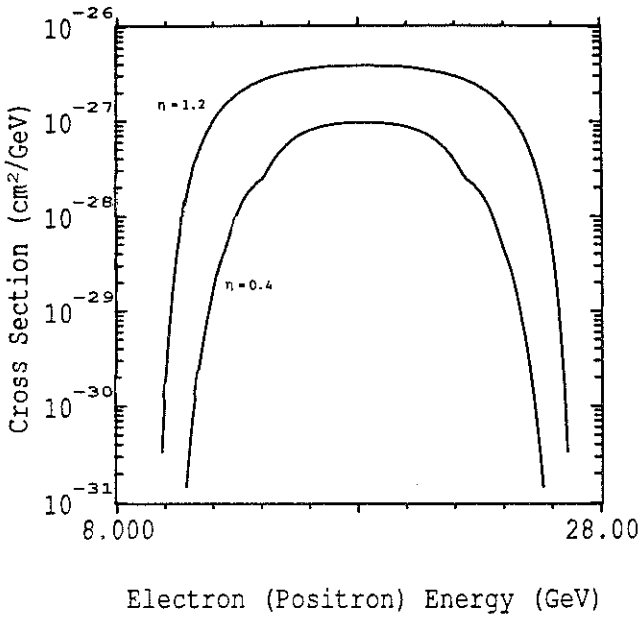

Figure 8: Differential cross-section *vs.* electron (or positron) energy for pair production when 36.5-GeV photons are incident on a $\lambda = 350$ nm laser pulse. Lower curve: intensity parameter $\eta = 0.4$; upper curve: intensity parameter $\eta = 1.2$.

pulses or 10^4 pairs in one day, which is more than sufficient to establish the cross section and study the low end of the mass spectrum.

6 The e^+e^- Mass Spectrum in High Fields

In Fig. 9 we show the effective mass of the e^+e^- pairs as observed at the Darmstadt experiments [4]. If these peaks are due to a strong-field QED process they should be reproduced in the proposed measurement. The apparatus and layout are the same as in the previous measurement of the low-end part of the spectrum. The principal difference is that to reach high masses (up to 2 MeV) we must have sufficient probability for the absorption of $n \gtrsim 8$ photons. Thus the intensity parameter of the laser beam will have to be set at $\eta \gtrsim 1$.

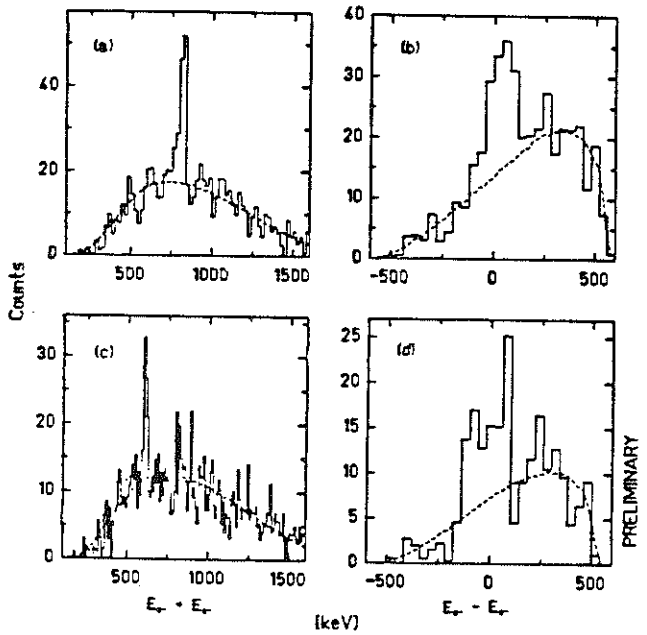

Figure 9: Results of a preliminary analysis of U + Th collisions near 5.87 MeV/c [4]. The $(E_{e+} + E_{e-})$ projections are for two subsets of data gated on beam energy, heavy-ion scattering angle and e^+ or e^- TOF chosen to enhance the prominent sum lines at $\sim$ 810 keV and $\sim$ 620 keV, respectively.

Figure 10 shows that rate of pair production per 36.5-GeV photon as a function of the electron (or positron) lab energy for seven laser-pulse energies: 0.01, 0.03, 0.1, 0.3, 1, 3, and 10 Joules. In all cases a lens with $f/D = 3$ is assumed, and we suppose that the high-energy photon beam has a radial σ of 60 μm as discussed in Sec. 2 and the Appendix. The spectra are narrower than the beam energy as the production is close to threshold and the electrons are nonrelativistic in the pair rest frame.

The invariant mass of the pair, when it is still in the laser field, is given by

$$\overline{M} = \sqrt{s} = 2\sqrt{n\omega_0\omega} = 0.75\sqrt{n}\ \mathrm{MeV}/c. \tag{30}$$

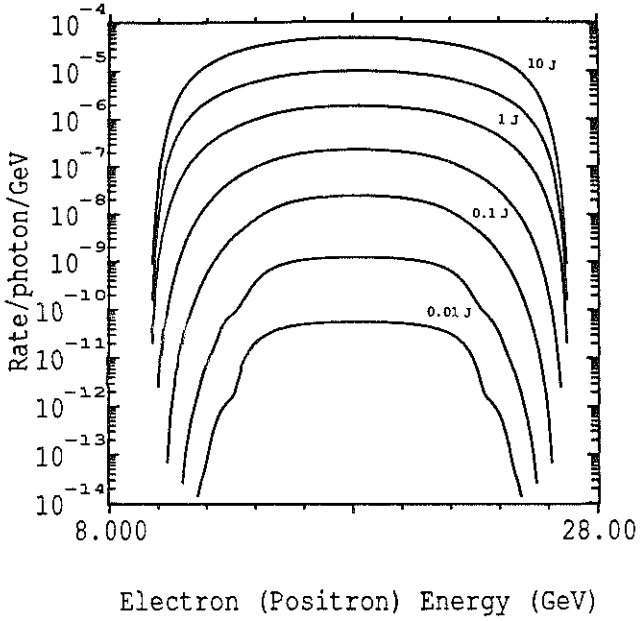

Figure 10: The calculated rate of pair production in collisions of a 36.5-GeV photon with a laser beam of 3.5-eV photons, as a function of the energy of the produced electron (or positron). The laser is focused in a lens of $f/D = 3$, and the high-energy photon beam has a radial σ of 60 μm. The seven curves are, from bottom to top, for 0.01, 0.3, 0.1, 0.3, 1, 3, and 10 Joule laser-pulse energies. Corresponding to these are $\eta_{max} = 0.21$ 0.37, 0.67, 1.16, 2.12, 3.68, 6.71, and $\Upsilon_{max} = 0.11$, 0.18, 0.33, 0.58, 1.05, 1.82, and 3.32, respectively.

That is, a line spectrum of pair masses is produced, depending on the number n of laser photons absorbed. The pair-production rate as a function of the number of laser photons absorbed is shown in Fig. 11 for seven laser-pulse energies.

A complication arises in interpreting the mass spectrum because the e^+e^- are produced in a strong field where the effective mass of the electrons is $\overline{m} = m\sqrt{1+\eta^2}$, and its 4-vector is modified to be

$$\overline{p} = p + \kappa\omega_0, \qquad \kappa = \frac{m^2\eta^2}{2(\overline{p}\cdot\omega_0)} \tag{31}$$

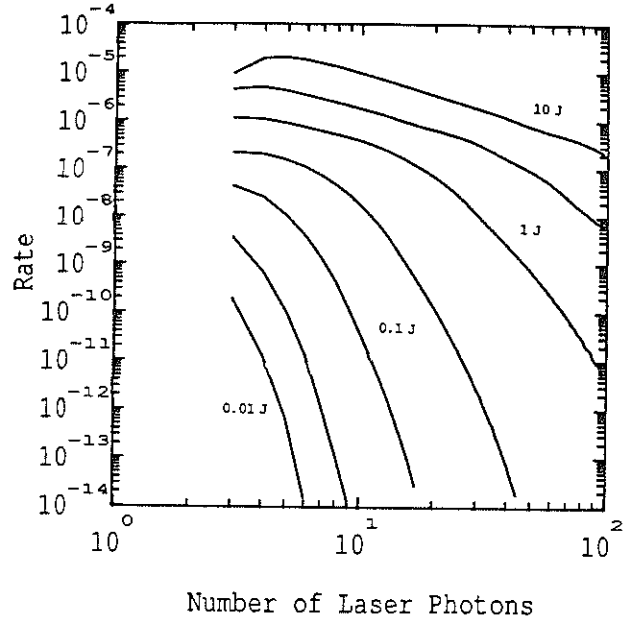

Figure 11: The calculated rate of pair production as a function of number of laser photons, for the conditions of Fig. 10.

with ω_0 the laser-photon 4-vector. As a result the effective mass of the pair in the strong field is

$$\overline{M}^2 = (\overline{p}_1 + \overline{p}_2)^2 \tag{32}$$

In case of symmetric production the invariant mass observed outside the laser beam is

$$M^2 = (p_1 + p_2)^2 = \overline{M}^2 - 4m^2\eta^2 \tag{33}$$

whereas for forward/backward production

$$M^2 = \overline{M}^2/(1+\eta^2) \tag{34}$$

If we write in general

$$\overline{M}^2 = 4m^2(1+\eta^2+\Delta) \quad . \tag{35}$$

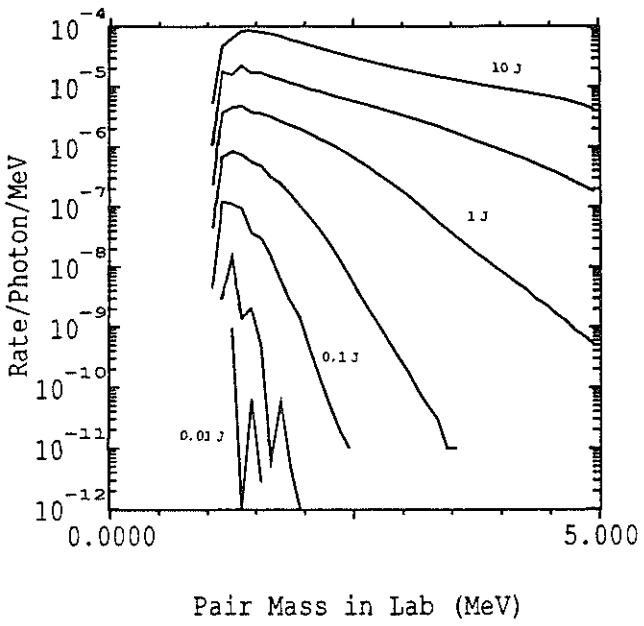

Figure 12: The calculated rate of pair production as a function of the pair mass as measured in the laboratory, for the conditions of Fig. 10. The intrinsic line spectrum is smeared into a continuum as the electrons leave the strong-field region.

Then the corresponding M^2 once the pair leaves the strong field will vary over the range

$$1 + \frac{\Delta}{1+\eta^2} \leq \frac{M^2}{4m^2} \leq 1 + \Delta. \tag{36}$$

In the limit of large η, the lower limit of the range is just $M = 2m$ no matter what the value of $\overline{M}$! If it appears that the physics requirement is for good mass resolution in $\overline{M}$ rather than M, it may be necessary to restrict the experiment to nearly symmetric decays. Experimental reality may force this requirement anyway, since one member of an asymmetric pair always lies closer to the unscattered beam than for a symmetric pair, and detection is simpler in the symmetric case.

Figure 12 shows the rate of pair production as a function of the pair mass as observed outside the high-field region, for seven laser-pulse energies. At very low laser field strengths the invariant mass is little affected by the laser, and the line spectrum can still be discerned. At large field strengths the intrinsic line spectrum will be smeared into a continuum. We see that laser-pulse energies of order 1 Joule would be advantageous to study pair masses near 2 MeV/c^2.

Departures from the QED prediction [16] might then arise in two ways. The intrinsic line spectrum might not be as expected, or the smearing of that line spectrum into the laboratory continuum might be altered. While a single run as proposed might be sufficient to reveal the second effect, a scan of primary electron-beam energies would be required to explore the first effect.

> Another potential loss of mass resolution is Compton scattering of the electron or positron before they leave the strong-field region of the laser beam. This effect increases as η^2 and a possible way to circumvent it is to use only events where the electron and positron energies add up to the beam energy.

If a laser pulse of one Joule is used, the total pair rate per high-energy photon is about 10^{-5} according to Fig. 10. We saw in Sec. 2 that if 0.1 Joule of laser light is used to create the high-energy photons then about 3×10^5 of these would be produced in a 9% energy bite. Then the total pair rate would exceed one per pulse, and the overlapping pairs could not be analyzed. The laser intensity at the first interaction point should be reduced to perhaps 10 mJoule to keep the pair rate to 1/3 per pulse. With 1-Hz laser operation some 25,000 pairs could be collected per day.

If the laser achieves only 0.1-Joule pulses then the pair rate is only about 10^{-7} per γ, and there would be only about 1/50 pair per pulse. Even so, about 1500 pairs could be collected per day. Thus a 10-day run would be sufficient for this measurement.

7 The Laser System

We have built a laser system capable of delivering 1-Joule pulses of infrared light at $\lambda = 1.05$ μm [18] with the system presently operating at the 30-mJ level [13]. A laser pulse from a mode-locked oscillator is frequency chirped, temporally expanded in a fiber, and further stretched in time by an expansion grating pair. The longer pulse allows more energy to be extracted from the subsequent amplifier system than would be by a short pulse. After amplification, the pulse is compressed by a grating pair to picosecond or subpicosecond duration. There is a resulting increase in power equal to the chirp ratio, the stretched-pulse duration divided by the compressed-pulse duration. The chirping in the fiber, the compression and expansion grating pairs, and the chirp ratio are well described in the literature [19].

A schematic diagram of the present CPA laser system is shown in Fig. 13. It consists of three parts: the pulse-preparation stage, the amplifier chain, and the compression stage. Figure 13(a) shows the pulse-preparation stage. A cw-pumped mode-locked Nd:YLF oscillator generates a 100-MHz train of 50-ps pulses at a wavelength of 10530 Å. The pulses are coupled into a 0.8-km single-mode optical fiber with a 9-μm core and then sent through a pair of expansion gratings. Due to self-phase modulation and group-velocity dispersion in the fiber, and further dispersion by the expansion grating pair, the pulses are chirped to approximately 300 ps across a 37-Å bandwidth. A single nanoJoule-energy pulse is selected by a Pockels cell and seeded into a Q-switched, end-mirror-dumped regenerative amplifier. The amplifier uses a 7-mm-diameter phosphate Nd:glass rod (Kigre Q98). (A carefully designed regenerative amplifier not only amplifies the laser pulse but also shapes the laser spectrum. For this reason, the regenerative amplifier is considered part of the pulse-preparation stage.) A 1-mJ pulse is selected from the pulse train, which is transmitted through the 50% reflective end mirror in the regenerative amplifier. The spatial profile of the beam is cleaned with an air spatial filter. An attenuator consisting of a half-wave plate between two polarizers is used to control the energy input to the amplifier chain. The cw autocorrelator monitors compressed pulses before amplification. The compression is done with a small compression grating pair, which is matched to the compression gratings after the amplifier chain.

The amplifier chain and the compression stage are shown in Fig. 13(b). The amplifier chain consists of a double-pass 9-mm-diameter amplifier (Kigre Q-98, 235 mm long), and a single-pass 16-mm-diameter amplifier (Hoya LHG-8, 360 mm long). A single-pass 30-mm-diameter amplifier (Hoya LHG-8, 360 mm long) will be added when compression gratings with a higher damage threshold are installed. One Pockels cell after the 9-mm amplifier further isolates the pulse and suppresses any feedback pulse, which may result from reflections off optical elements. An additional attenuator increases the system's dynamic range to 10^6. A vacuum spatial filter after each amplifier is used to upcollimate, image relay, and spatially filter the pulse. The energy of the chirped pulse after the 16-mm amplifier can be as high as a Joule with a repetition rate of 1 shot per 70 sec (limited by the thermal lensing in the 16-mm amplifier rod).

The compression stage consists of two 1700-line/mm gold-coated holographic gratings, with dimensions 80×110 mm. The gratings are used in the near-Littrow, double-pass configuration with a separation distance of 164 cm. The laser pulse is compressed to 1.6 ps with a bandwidth of 13.5 Å when no saturable absorber is used. The laser beam has a 36-mm diameter limiting the maximum energy to 300 mJ currently, due to the damage threshold of the compression gratings. An autocorrelator and an energy meter are used to measure the final pulse width and pulse energy after compression. A saturable absorber has been used to clean up the pulse wings and produce a 0.9-ps

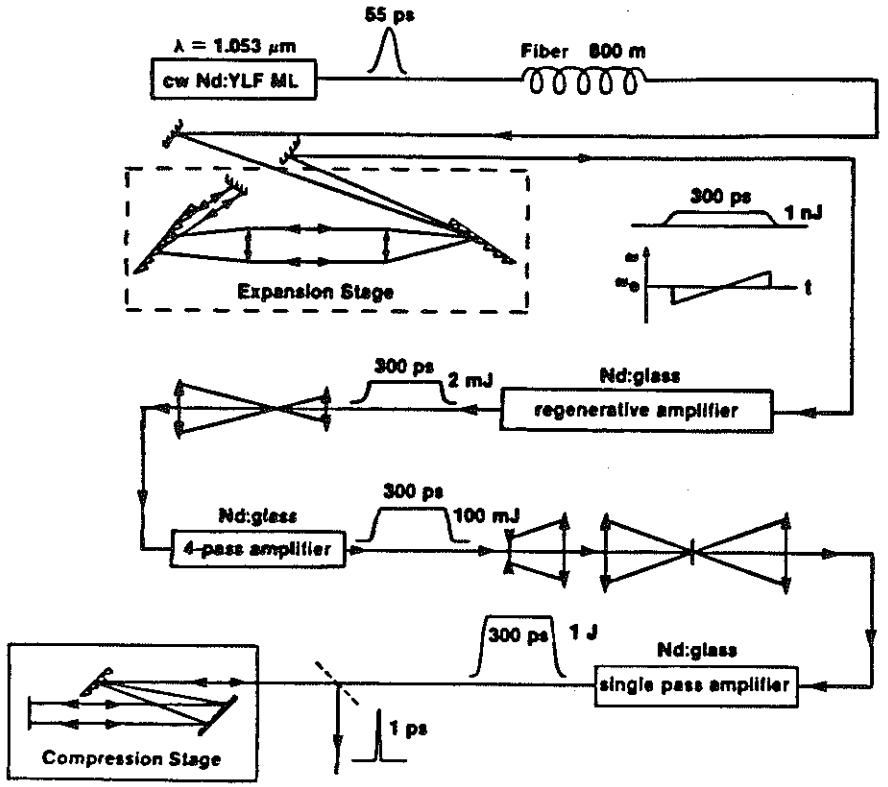

Figure 13: Chirped pulse amplification and compression. A pulse from the mode-locked oscillator is chirped in a fiber and amplified before being compressed to a pulselength of less than 2 psec.

Gaussian laser pulse when this is necessary. The autocorrelation trace of the pulse is shown in Fig. 14.

With the compression gratings currently in the system, we are limited to laser pulse energies of $\sim$ 100 mJ to avoid damage. With new 16 × 25 cm gratings and with the addition of an upcollimator, we will be able to take advantage of our full amplification capabilities, and produce laser energies in excess of 1 J and intensities

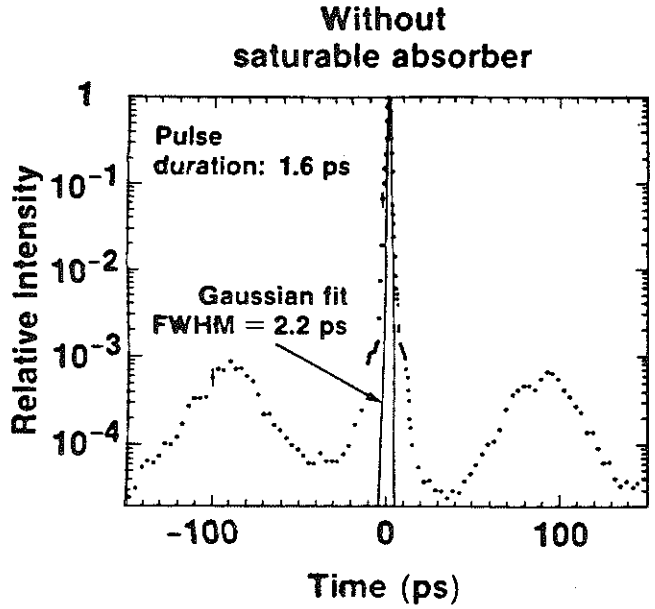

Figure 14: Autocorrelation trace of the compressed pulse. Assuming a gaussian profile, this measurement corresponds to a pulsewidth of 1.6 picoseconds. Note the logarithmic scale.

significantly in excess of 10^{19} W/cm^2.

The limitation of the present system is its repetition rate. However, a large-aperture, high-gain, slab-geometry, Nd:glass amplifier has been designed, constructed, characterized, and routinely operated at the University of Rochester. This amplifier was specifically designed to provide high-energy (~3 J), 0.3-1.0-ns pulses at medium repetition rate (2 Hz) with the superior beam quality (both phase and polarization) required for efficient frequency *tripling*. These requirements are an excellent match to the chirped-pulse amplification stage of our present laser system. This amplifier has been in operation for over one year with in excess of 200,000 shots delivered. We propose to duplicate this proven design, using it to replace the repetition-rate-limiting final amplifier stages of the current laser system.

At the University of Rochester Laboratory for Laser Energetics tripling of nanosecond IR pulses (resulting in $\lambda = 350$ nm) has been accomplished with efficiency $\sim 80\%$

[20]. We have performed some experiments based on the theory of ref. [21] and have observed 75% efficiency for frequency doubling of a 1-ps laser pulse. In addition recent work in Rochester has shown high third-harmonic conversion efficiency of broadband pulses by angularly dispersing the beam in the crystal and then recollimating it. We can use this approach if we elect to frequency triple before compressing. This approach, which would guarantee high efficiency, involves the use of UV gratings which are now becoming commercially available.

8 Appendix: The e-ω and γ-ω Interaction Regions

We examine here in greater detail the optimum focusing of the electron and laser beams in the Breit-Wheeler experiment. The discussion includes the emittance of the electron beam as well as the scattering angle of the high-energy γ's with respect to the electrons.

The laser spot at the second (γ-ω) interaction point must be only a few wavelengths across to maintain the highest possible electric field. If a high-energy γ is produced by a Compton scatter in the first (e-ω) interaction at a radius r_1 from the beam axis, it must have lab angle $-r_1/L$ to arrive usefully on axis at the second interaction point, which is distance L downstream. The lab angle is compounded of the scattering angle θ, and the slope r' of the incident electron. To arrive at $r = 0$ at the second interaction point, a γ should have scattering angle $\theta = -r_1/L - r' = -(r_1 + r'L)/L = -r_2/L$, where r_2 is the position of the electron at the second interaction point if it had not scattered. Thus the electron beam size at the second interaction point should be

$$\sigma_{r_2} = L\Delta\theta \approx 60\ \mu\text{m}$$

when $L = 10$m, and $\Delta\theta = 60\ \mu$rad is the desired acceptance in Compton scattering angle as considered in Sec. 2 above.

The electron beam is, in general, focused at a distance z upstream of the second interaction point. If the beam has emittance ϵ and the focusing system is described by the strength β^*, we have

$$\sigma_{r_2}^2 = \epsilon\beta^*\left(1 + \frac{z^2}{\beta^{*2}}\right).$$

The electron beam size at the first interaction point, distance L upstream, is related by

$$\sigma_{r_1}^2 = \epsilon\beta^*\left(1 + \frac{(L-z)^2}{\beta^{*2}}\right).$$

For given ϵ and L, both β^* and z are to be optimized.

From Eq. (12) for the luminosity of the Breit-Wheeler experiment, we see that we should minimize the product of the area of the electron-beam spot at the first interaction point and the area of the high-energy photon beam at the second interaction point. The latter area is larger than that of the electron beam there due to Compton scattering. We can write

$$A_{\gamma_2} = \pi(\sigma_{r_2}^2 + \theta(E)^2),$$

where θ is the Compton scattering angle for γ's of energy E. For $E = E_{\max}$, $\theta = 0$; while for $E = E_{\min}$ given by Eq. (10), $\theta = \Delta\theta = \sigma_{r_2}/L$ by definition. In any case, the size of the γ beam at the second interaction point is linked to the size of the electron beam there, and not directly to the size of the electron beam at the first interaction point. So once the size of the electron beam at the second interaction point is fixed, the luminosity is a minimum when the electron spot at the first interaction point is also a minimum.

To effect this minimization we use the method of Lagrange multipliers, forming the function

$$f(\beta^*, z) = \sigma_{r_1}^2 + \lambda\sigma_{r_2}^2$$

where λ is the multiplier. The minimum of f is at

$$\beta^* = \frac{L\sqrt{\lambda}}{1+\lambda}, \qquad z = \frac{L}{1+\lambda},$$

and the constraint that $\sigma_{r_2} = L\Delta\theta$ implies that

$$\lambda = \frac{\epsilon^2}{L^2\Delta\theta^4}.$$

The optimum size of the electron beam at the first interaction point is then

$$\sigma_{r_1} = \frac{\epsilon}{\Delta\theta}.$$

For our standard example that

$$\epsilon = 3 \times 10^{-10} \text{ m-rad}, \qquad L = 10 \text{ m}, \qquad \Delta\theta = 6 \times 10^{-6},$$

we then have

$$\sigma_{r_1} = 50\ \mu\text{m}, \qquad \sigma_{r_2} = 60\ \mu\text{m}, \qquad \lambda = 0.7, \qquad z = 5.9 \text{ m}, \qquad \beta^* = 4.9 \text{ m}.$$

The corresponding angular divergence of the electron beam is

$$\sigma_\theta = \sqrt{\epsilon/\beta^*} = \Delta\theta\sqrt{1 + (\epsilon/L\Delta\theta)^2} \approx \Delta\theta = 6 \times 10^{-6}.$$

To utilize high-energy photons of energies down to $E_{\min}$ in the γ-ω interaction, the laser spot size at the first interaction point should be of size σ_{r_1} also.

9 References

[1] J. Schwinger, Proc. Nat. Acad. Sci. **40** (1954) 132.

[2] For a review see K.T. McDonald, "Proposal for Experimental Studies of Nonlinear Quantum Electrodynamics", Princeton U. Report DOE/ER/3072-32 (Sept. 1986).

[3] See for instance Sec. 40 of V.R. Berestetskii, E.M. Lifshitz and L.P. Pitaevskii, "Quantum Electrodynamics," 2nd ed., (Pergamon Press, 1982).

[4] See for instance T. Cowan and J. Greenberg, in "Physics of Strong Fields," ed. W. Greiner (Plenum, N.Y. 1987); the original papers are J. Schweppe *et al.*, Phys. Rev. Lett. **51** (1983) 2261; T. Cowan *et al.*, Phys. Rev. Lett. **56** (1986) 444; P. Salabura *et al.*, Phys. Lett. **B245** (1990) 153; W. Koenig *et al.*, Phys. Lett. **B218** (1989) 12.

[5] A. Belkacem *et al.*, Phys. Lett. **B177** (1986) 211; Phys. Lett. **B206** (1988) 561; R. Medenwalt *et al.*, Phys. Lett. **B227** (1989) 483.

[6] R.C. Fernow *et al.*, "Proposal for an Experimental Study of Nonlinear Compton Scattering," Princeton U. Report DOE/ER/3072-55 (Oct. 25, 1989).

[7] See for instance M. Bell and J.S. Bell, Part. Acc. **24** (1988) 1; R. Blankenbecler and S.D. Drell, Phys. Rev. Lett. **61** (1988) 2324; M. Jacob and T.T. Wu, Nucl. Phys. **B303** (1989) 389.

[8] G. Breit and J.A. Wheeler, Phys. Rev. **46** (1934) 1087.

[9] R.H. Milburn, Phys. Rev. Lett. **10** (1963) 75; I.F. Ginzburg, G.L. Kotkin, V.G. Serbo and V.I. Telnov, Nucl. Inst. and Meth. **205** (1983) 47 and references therein to earlier work.

[10] H.R. Reiss, Phys. Rev. Lett. **26** (1971) 1072.

[11] H. Tsertos *et al.*, Phys. Rev. D **40** (1989) 1397; S.M. Judge *et al.*, Phys. Rev. Lett. **65** (1990) 972.

[12] A.L. Hallin *et al.*, "A Sensitive Search for Resonances in Low Energy e^+e^- Scattering," Princeton U. preprint (May, 1991).

[13] S.L. Adler, Phys. Lett. **B221** (1989) 39.

[14] J.E. Spencer, "High Brightness Sources for Colliders," SLAC-PUB-5561 (May 1991).

[15] See for instance A.C. Melissinos, "Final Technical Report Grant AFOSR-87-0328," University of Rochester (1991); C. Bamber, W. Donaldson, T. Juhasz, L. Kingsley and A.C. Melissinos, Part. Acc. **23** (1988) 255.

[16] N.B. Narozhnyi, A.I. Nikishov and V.I. Ritus, Soviet Physics JETP **20** (1963) 622; see also Sec. 101 of Ref. [3].

[17] P. Chen and K. Yokoya, Phys. Rev. Lett. **61** (1988) 1101.

[18] J.Y. Hemery, F. Lemeilleur and G. Von Holtey, CERN/LEP-BI/86-6 report; S. Pensoti *et al.*, Nucl. Instr. and Methods **A257** (1987) 538.

[19] P. Chen and V.I. Telnov, Phys. Rev. Lett. **63** (1989) 1796.

[20] P. Maine, D. Strickland, P. Bado, M. Pessot, and G. Mourou, IEEE J. Quantum Electron. **QE-24**, 398 (1988).

[21] R.S. Craxton, Optics Comm. **34** (1980) 474; W. Seka, S.D. Jacobs, J.E. Rizzo, R. Boni and R.S. Craxton, Optics Comm. **34** (1980) 469.

[22] Y. Wang and R. Dragila, Phys. Rev. A **41** (1990) 5645.

REPORT OF THE GROUP ON BEAM-BEAM EFFECTS IN CIRCULAR COLLIDERS*

MIGUEL A. FURMAN
Accelerator and Fusion Research Division
Lawrence Berkeley Laboratory
University of California
Berkeley, CA 94720, U.S.A.

ABSTRACT

We present a summary of the discussions and conclusions of the working group on beam-beam effects for circular colliders. This group was part of the larger beam-beam dynamics group at the 7th ICFA Workshop on Beam Dynamics, on the subject "Beam-Beam and Beam-Radiation Interactions," held at UCLA, May 13–16, 1991.

1. Summary of Issues Considered

There were discussions on two topics: new collider design, and simulation issues. In the first category, Ivanov[1] gave a presentation on Novosibirsk's ϕ factory project, a 510 MeV $\times$ 510 MeV machine with a peak luminosity of (3–10) $\times 10^{33}$ cm^{-2} s^{-1}, scheduled to be completed in 1997. He also mentioned an asymmetric B factory, a 4 GeV $\times$ 7 GeV machine with a luminosity of 5×10^{33} cm^{-2} s^{-1}.

Most of the time spent by the group was devoted to discussions on beam-beam simulation issues. Ivanov's talk on the ϕ factory included a section on simulation results. Hirata[2] gave a talk, at a plenary session of the workshop, emphasizing the coherent modes approach to the beam-beam problem. Furman[3] presented results on beam-beam simulations for the proposed SLAC/LBL/LLNL B factory, a 3.1 GeV $\times$ 9 GeV machine with a luminosity of 3×10^{33} cm^{-2} s^{-1}. Koga[4] presented results of a study performed with a one-dimensional particle-in-cell code (PIC) for the SSC. Irwin[5] briefly described an "acceleration" algorithm that allows one, in principle, to shorten considerably the simulation time required to study the development of tails in a beam. Ziemann[6] gave a talk on generalizations of the Bassetti-Erskine[7] calculation of the electric field produced by a modified Gaussian charge distribution (Gaussian $\times$ polynomial, with rotated axes) in the context of applications to single-pass colliders such as the SLC. A simulation issue of long-bunch effects was brought up by Ivanov in his talk, emphasizing the detrimental effect of the longitudinal electric field; the importance of this effect was apparently first pointed out by Derbenev and Skrinsky;[8] more recently it has been addressed by Hirata *et al.*[9]

* Work supported by the Director, Office of Energy Research, Office of High Energy and Nuclear Physics, High Energy Division, of the U.S. Department of Energy under Contract no. DE-AC03-76SF00098.